PET AND CT IMAGE REGISTRATION OF THE RAT BRAIN AND SKULL USING THE AIR ALGORITHM

J. J. Vaquero[1], M. Desco[2], J Pascau[2], A. Santos[3], I. J. Lee[1], J. Seidel[1] and M. V. Green[1]

[1] National Institutes of Health, Bethesda, Maryland 20892

[2] Hospital Universitario Gregorio Marañón, Madrid, Spain

[3] Universidad Politécnica de Madrid, Spain

Abstract

Spatially registered PET and CT images of the same small animal offer at least three potential advantages over PET alone. First, the CT images should allow accurate, nearly noise-free correction of the PET image data for attenuation. Second, the CT images should permit more certain identification of structures evident in the PET images and third, the CT images provide *a priori* anatomical information that may be of use with resolution-improving image reconstruction algorithms that model the PET imaging process. Thus far, however, image registration algorithms effective in human studies have not been characterized in the small animal setting. Accordingly, we evaluated the ability of the AIR algorithm to accurately register PET F-18 fluoride and F-18 FDG images of the rat skull and brain, respectively, to CT images acquired following each PET imaging session. The AIR algorithm was able to register the bone-to-bone images with a maximum error of less than 1.0 mm. The registration error for the brain-to-brain study, however, was greater (2.4 mm) and required additional steps and user intervention to segment the brain from the head in both data sets before registration. These preliminary results suggest that the AIR algorithm can accurately combine PET and CT images in small animals when the data sets are nearly homologous, but may require additional segmentation steps with increased mis-registration errors when registering disparate, low contrast soft tissue structures.

I. INTRODUCTION

Imaging technologies originally developed for use in human medical diagnosis are rapidly being adapted to imaging small animals such as the mouse and rat [1]. Moreover, it has become increasingly apparent that certain combinations of these method can yield synergistically improved results. The combination of PET and CT, for example, offers the prospect of nearly noise-free attenuation correction of the PET data, improved target identification and the potential for correcting PET data for other confounding effects, e.g. positron range variations. Before these benefits can be realized, however, the PET and CT image data must be in spatial registration. While a number of multi-modality registration algorithms have been devised and validated in human subjects, comparatively little is known about the performance of these algorithms when applied to PET and CT images of small animals. Accordingly, we have begun investigating already validated human registration algorithms to establish their accuracy in this setting. As an initial test, we elected to evaluate the automated image registration, or "AIR" algorithm [2] in two extreme cases, high contrast bone-to-bone registration of CT and F-18 fluoride PET images of the rat head and low contrast brain-to-brain registration of F-18 FDG and CT images of the rat head.

II. MATERIALS AND METHODS

Both experiments were carried out in a similar manner using the rat head as the imaging target. In each study the rat was injected intravenously with the PET tracer (1.3 mCi of F-18 fluoride and 2.8 mCi of F-18 FDG) and uptake allowed to occur with the animal awake. At the end of the uptake period (2 hours for F-18 fluoride and 1 hour for F-18 FDG) the animal was sacrificed and the head removed intact. Each head was packed snugly into a plastic tube having almost exactly the head diameter. After adding extra gauze to immobilize the head within the tube, the tube was sealed. Three glass capillary tubes partially filled with an F-18 solution were then taped to the sides of the tube. These partial line sources were oriented axially along the tube and were spaced at roughly equal angular intervals around the tube circumference with a fourth, shorter tube placed midway along the tube length. These tubes with attached line sources were then affixed to the mechanical rotation stage of the "PiPET" small animal PET scanner [3] and imaged for several hours in order to acquire large numbers of counts (16 M counts for F-18 fluoride and 44 M counts for F-18 FDG). These data were then reconstructed with FBP and ramp filter into forty-three 64 x 64 tomographic images that spanned the axial field-of-view. Spatial resolution in these images is approximately 1.8 mm (isotropic).

Following each PET study, the tubes were transported to a GE High Speed CT/i human CT scanner where the entire head was again imaged using the same CT settings (80 kVp, 100 mA, 1 mm thick slices, 96 mm x 96 mm in-plane FOV, 512x512 acquisition matrix).

After removing extraneous markers, the PET and CT volumetric data sets obtained in each study were registered with the AIR algorithm [2] using an implementation previously validated in human clinical studies [4]. Registrations were done using a rigid geometric transformation (six parameters) and no smoothing of either data set. For the case of F-18 fluoride and CT, the studies were treated as an intramodality registration since the CT and PET images showed a strong correlation between their intensity distributions. In contrast, The F-18 FDG and CT studies required manual intervention to segment the brain in both studies prior to registration. The algorithm in this case was applied not to the original greyshade images but to the homogeneous regions obtained from the segmentation masks. This semi-automated, user-validated segmentation process was needed, in part, because high FDG uptake structures are present in the FDG-labeled rat head that are not present in FDG images of the human head, e.g. the Harderian glands.

In both of these registration tasks, the "gold standard" was taken to be the position of 12 to 15 pairs of homologous points identified manually along the fiducial lines attached to the tubes. An estimate of the registration error after applying the

0-7803-6503-8/01/$10.00 2001 IEEE

AIR algorithm was obtained following the methodology described by West et al. [5]. Differences found between the gold standard and the AIR algorithm in translation are the same throughout the registered images whereas the rotational error increases away from the center. As a result, we calculated the maximum registration error and the mean registration error over the entire brain volume.

III RESULTS

F-18 fluoride vs. CT. In this case, the automatic algorithm was robust and relatively insensitive to algorithm settings. The maximum registration error within the brain volume was less than 1.0 mm. Images illustrating this bone-to-bone registration are shown in Figure 1.

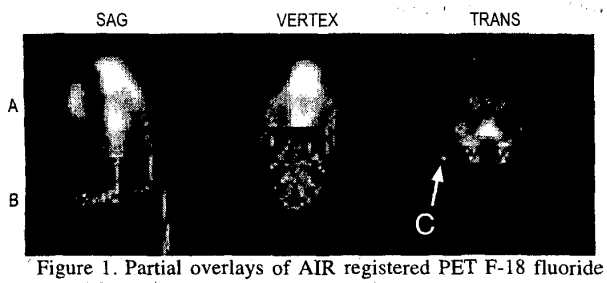

Figure 1. Partial overlays of AIR registered PET F-18 fluoride (A) and CT bone images (B). Note continuity of bones across the PET and CT image boundaries. C=capillary tube.

F-18 FDG vs. CT. In this case, the algorithm was unstable and could not be used until all non-brain structures were removed from both studies. Maximum mis-registration in this case was 2.4 mm with an average mis-registration of 2.1 mm. Images illustrating this brain-to-brain registration are shown in Figure 2.

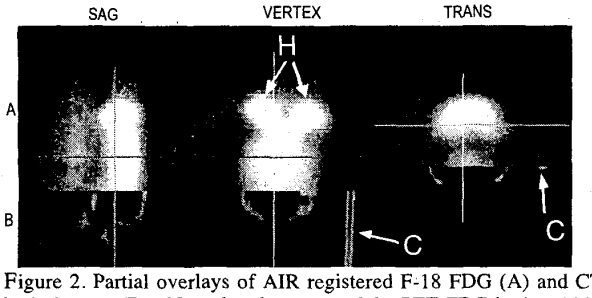

Figure 2. Partial overlays of AIR registered F-18 FDG (A) and CT brain images (B). Note the placement of the PET FDG brain within the CT skull. H=Harderian glands, C=capillary tube.

IV. DISCUSSION

The combination of PET and CT images of the same animal should improve PET target identification, attenuation correction and provide additional information that may be useful in improving PET study quality. In some circumstances it may be necessary to register these data spatially without external fiducial markers, a situation in which alignment might depend strongly on image content. The two cases studied here represent extreme versions of this situation, one in which homology between the sequences is nearly total (bone-to-bone) and the other a situation (brain-to-brain) where only the surface shapes of the structures to be registered are similar. As might be expected, registration errors were larger for the latter case than for the former by more than a factor of two. Given the great variability in the appearance of PET images of the brain for different tracers, it seems likely that registrations errors will also be variably large and, in all probability, tracer-dependent.

The failure of the automated features of the AIR algorithm in the brain-brain registration case is also noteworthy. The AIR algorithm was developed for multi-modality imaging in human subjects and contains default settings tailored to this application. In the present case, the rat head contains structures not present in humans, but which concentrate FDG more strongly than the brain. Unless these structures are removed by segmentation, the AIR algorithm cannot successfully register the PET and CT brain images. Thus, it may be that additional segmentation steps will have to be devised on a tracer-by-tracer basis to eliminate extreme anatomical and/or functional differences that exist between human and small animal studies.

Despite these complications, the present study does suggest that the AIR algorithm can register PET images of the skull and brain to CT images of the head with reasonable accuracy. Further studies, using improved fiducial markers to better assess registration accuracy and lower kVp to improve CT soft tissue contrast, will be required to determine to what degree this finding can be generalized to other tracers and organs.

V. CONCLUSIONS

The AIR registration algorithm, developed for use in multi-modality image registration in human subjects, can be used to automatically register CT with F-18 fluoride bone images of the rat head. PET FDG images of the brain can also be registered with CT but only after modifications that require user-intervention and that yield larger registration errors. Further studies are required to establish the generality of this approach for different tracers and for variations in each imaging procedure.

VI. ACKNOWLEDGEMENT

The authors thank Marlene Skopec for her valuable assistance in performing the CT studies.

VII. REFERENCES

[1] M. J. Paulus, H. Sari-Sarraf, S. S. Gleason, M. Bobrek, J. S. Hicks, D. K. Johnson, J. K. Behel, and L. H. Thompson, "A New X-ray Computed Tomography System for Laboratory Mouse Imaging", *IEEE Trans Nucl Sci*, vol. 46, no. 3, pp. 558-564, 1999.

[2] R. P. Woods, J. C. Mazziotta, and S. R. Cherry, "MRI-PET Registration With Automated Algorithm", *Journal of Computer Assisted Tomography*, vol. 17, no. 4, pp. 536-546, 1993.

[3] S. Siegel, J. J. Vaquero, L. Aloj, J. Seidel, W. R. Gandler, and M. V. Green, "Initial Results from a PET/Planar Small Animal Imaging System", *IEEE Trasn Nucl Sci*, vol. 46, no. 3, pp. 571-575, 1999.

[4] M. Desco, J. Lopez, and C. Benito et al., *A Multimodality Workstation in Practice*, in Computer Assisted Radiology. Amsterdam: Elsevier Science, 1999.

[5] J. West, J. M. Fitzpatrick, M. Y. Wang, B. M. Dawant, et al., "Comparison and evaluation of retrospective intermodality brain image registration techniques", *Journal of Computer Assisted Tomography*, vol. 21, no. 4, pp. 554-566, 1997.

Three-Dimensional Geometric Sensitivity Calculation for Three-Headed Coincidence Imaging.

Y. D'Asseler[1], S. Vandenberghe[1], C.G. Matthews[2], M. Koole[1], R. Van deWalle[1], I. Lemahieu[1], R.A. Dierckx[3]

[1]Ghent University, Department of Electronics and Information Systems
Sint Pietersnieuwstraat 41, B-9000 Ghent, Belgium
[2]Marconi Medical Systems, 595 Miner Road, Cleveland, Ohio 44143, USA
[3]Ghent University Hospital, Division of Nuclear Medicine
De Pintelaan 185, B-9000 Ghent, Belgium

Abstract

Several manufacturers offer two-headed coincidence imaging with their gamma camera systems. To improve sensitivity, three-headed coincidence imaging has been proposed. In an earlier work, we investigated how the two-dimensional sensitivity varies in the field of view of such a system. In this paper, these calculations are extended to three dimensions, taking into account the finite axial length of the detector. The extension to three dimensions becomes particularly important when one acquires data in fully 3D mode, without using axial septa. The calculation of the three-dimensional sensitivity in a certain voxel consists of the integration of the axial sensitivity angle over the transaxial rotational weights corresponding to the lines of response (LORs) going through the voxel. This calculation is valid for any position of the camera, such as a U-shaped configuration or a triangular configuration. We have also investigated the use of axial septa by constraining the maximum axial incidence angle.

I. INTRODUCTION

Coincidence imaging with a gamma camera has raised a lot of interest over the last few years. For the moment, this type of imaging is usually done using a dual-headed camera. For this type of camera, the geometric sensitivity profile has been studied extensively. This sensitivity reaches a peak at the center of the Field Of View (FOV) and decreases practically linearly with increasing radial distance from the Center Of Rotation (COR) [1].

Recently, the possibility of triple-headed coincidence imaging has been discussed [2,3]. In this case, the geometric sensitivity depends on the configuration of the heads, the dimensions of the detectors and the distance from the center of the FOV. In an earlier work, we calculated the two-dimensional geometric sensitivity profiles for triple-headed coincidence detection [4]. In the two-dimensional case, the finite axial extent of the detector heads is not accounted for. This is an approximation which works reasonably well for the case of an acquisition with axial septa, effectively constraining the axial angle of incidence on the detector heads. When imaging without axial septa, however, the two-dimensional calculation is not accurate anymore, and a three-dimensional calculation is necessary.

In this work, we present a method for calculating the three-dimensional geometric sensitivity profiles for any triple-headed gamma camera configuration, and in fact, for coincidence imaging with any number of planar detector heads. These methods are then applied to a realistic camera configuration, based on the IRIX triple-headed gamma camera operating in fully-3D mode [5]. Three different configurations were investigated. Also, the use of axial septa was simulated.

II. METHODS

A. Calculation of Rotational Weights for a LOR

The calculation of the geometric sensitivity for coincidence imaging with a camera with more than two planar detector heads can be reduced to the case of two detector heads by considering each combination of two detectors separately. The difference with the case of conventional two-headed coincidence imaging is that the heads may have an arbitrary angle with respect to each other. After the calculation of the sensitivity for each head combination, the total sensitivity is obtained by summing the results of these calculations.

The first step in the three-dimensional sensitivity calculation is the calculation of the rotational weights of every Line Of Response (LOR). A LOR is defined here as a unique line in image space. It is detected by the camera if it goes through both detector heads. The rotational weight gives the angle over which the gamma camera can rotate while detecting the LOR.

In this work, we assume that the angular range of oblique LORs is limited by the edges of the detectors parallel to the axis of rotation, and not by the edges perpendicular to this axis. This means that, as the camera rotates, the path of the endpoint of the LOR on the detector heads will eventually encounter a detector edge parallel to the rotation axis. This

0-7803-6503-8/01/$10.00 2001 IEEE

assumption would hold for a detector system where the heads are part of a cylinder with the rotation axis as center, however, for planar detectors, it is a fairly good approximation [6]. However, one should keep in mind that this assumption no longer holds for the LORs with the largest axial angle of incidence.

Under the aforementionned assumption, the calculation of the rotational weights is reduced to a two-dimensional problem, as already addressed in earlier work [4]. Thus, the rotational weight of a LOR is only a function of its radial distance to the axis of rotation, and not of the oblique angle. In [4], rotational weights of LOR's are calculated for any two-dimensional detector configuration, as a function of the distance of the LOR to the axis of rotation and the orientations, radii and sizes of the detector heads.

B. Three-Dimensional Calculation of Geometric Sensitivity for a Pixel.

As the camera is rotated during image acquisition over an angle of 2π, we can assume rotational symmetry around the axis of rotation. Therefore, a pixel is described by two parameters: the axial distance from the center of the FOV z and the transaxial distance from the COR r, as defined in Fig. 1.

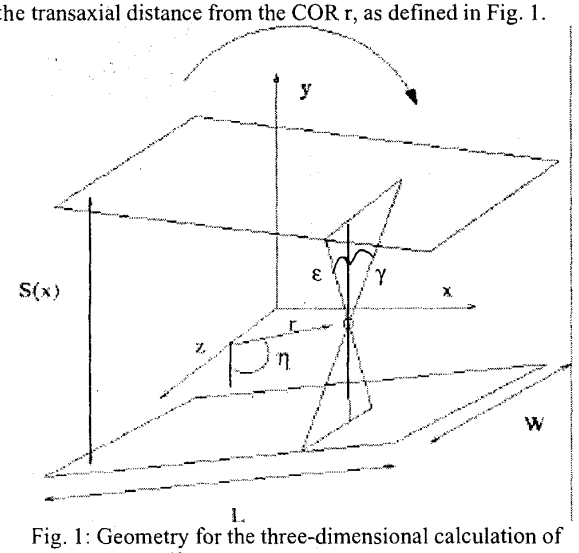

Fig. 1: Geometry for the three-dimensional calculation of sensitivity.

The sensitivity of a voxel is calculated as follows. We consider every LOR going through this voxel. According to our assumption, all LORs in a plane parallel to the axis of rotation and going through the pixel have the same rotational weight. The rotational weight of these LORs is given by the rotational weight of the LOR with a distance from the axis of rotation of $a=r\cos\eta$, η being the angle between the LOR under consideration which lies in the transaxial plane and a vertical reference axis in this plane (Fig. 1). For this LOR, the outer rotation angles of the camera, for which the LORs are still measured, are calculated: $\varphi_1(a)$ and $\varphi_2(a)$. Between these angles, the axial incidence angle limits ε and γ are integrated (Fig.1).

As the rotation angle of the camera varies, the effective distance between the detector heads along the LOR varies, which has its influence on the axial incidence angle limits. When the two detector heads are parallel, as in the case of dual-head coincidence detection, the effective distance between the detector heads for an angle φ is given by: $S(\varphi) = S_0 / \cos(\varphi)$ [1]. However, if the detector heads are no longer parallel, as in our case, the effective separation between the two detector heads becomes both a function of the distance from the COR, as well as of the angle φ. This is shown in Fig. 2. In this figure, rather than rotating the detector heads, we have chosen to rotate the LOR, tangent to the circle with as origin the COR and radius a, which is equivalent to camera rotation. An analytic expression of $S(a, \varphi)$ was found.

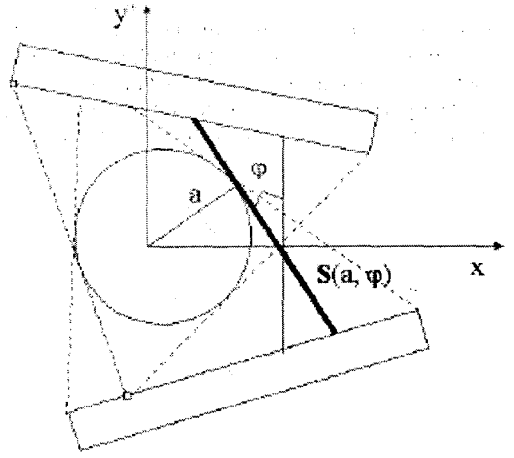

Fig. 2: Geometry for the calculation of $S(a, \varphi)$. The dashed lines indicate how far the detector can rotate while still detecting the LOR (angles φ_1 and φ_2).

Knowing $S(a, \varphi)$, ε and γ can be calculated as follows:

$$\varepsilon = \min\left\{\arctan\left[\frac{\frac{W}{2}+z}{\frac{S(a,\varphi)}{2}-r\sin\eta}\right], \arctan\left[\frac{\frac{W}{2}-z}{\frac{S(a,\varphi)}{2}+r\sin\eta}\right]\right\} \quad (1)$$

$$\gamma = \min\left\{\arctan\left[\frac{\frac{W}{2}-z}{\frac{S(a,\varphi)}{2}-r\sin\eta}\right], \arctan\left[\frac{\frac{W}{2}+z}{\frac{S(a,\varphi)}{2}+r\sin\eta}\right]\right\} \quad (2)$$

Once ε and γ are known, the geometric sensitivity of a pixel with axial distance to the COR z and radial distance to the COR r is given by:

$$w(r,z) = \int_{-\frac{\pi}{2}}^{\frac{\pi}{2}} \left[\int_{\varphi_2}^{\varphi_1} \{\varepsilon(r,z,\eta,\varphi)+\gamma(r,z,\eta,\varphi)\} d\varphi \right] d\eta \quad (3)$$

In this form

ula, the integration over η accounts for all transaxial angles that the LORs through the pixel can make with the vertical, whereas the integration over φ sums the axial sensitivity over the rotational weight of all LOR's with the same transaxial direction. Concerning the integration limits $\varphi_1(a)$ and $\varphi_2(a)$, it is important to notice that these limits actually fall apart in two regions, one on the left side of the COR and one on the right side, as indicated in Fig. 2. It is also important to notice that these integration limits depend on η through $a = r \cos(\eta)$. This means that the function $w(r,z)$ is in principle not separable into a transaxial and an axial component.

III. Results

We calculated the sensitivity maps for three different camera configurations. The first configuration was a regular dual-head setup. The second configuration was a U-shape consisting of this dual-headed setup, with one detector head added at the side, making a 90 ° angle with the other detectors. The last configuration was an equilateral triangle, where each detector head makes a 120° angle with the other heads (Fig. 3).

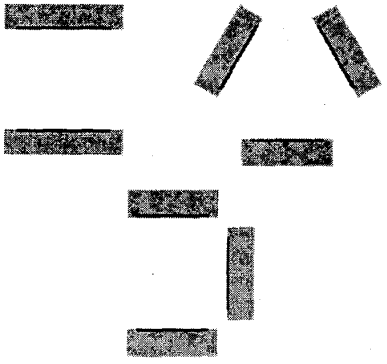

Fig. 3: Detector head configurations investigated.

The dimensions of the detector heads and the rotation radii were chosen to simulate the setup of the IRIX coincidence gamma camera (Marconi Medical). For this camera, the axial length is 387 mm, transaxial length 528 mm and radius of rotation was chosen to be 330 mm. For this rotation radius, in the U-shaped configuration the two opposed detector heads are shifted tangentially to the rotation circle with an amount of 40 mm away from the third head, to avoid collision of the heads with each other. This tangential shift was included in the calculations.

The results of the calculations are shown in Figures 4,5 and 6 for the dual-head, U-shaped and triangular configuration, respectively.

The sensitivity maps are calculated over the whole field of view: in the axial direction between the two edges of the camera and in the transaxial direction from the COR (at the center of the image) to the face of the crystal (radius of rotation). In a realistic case, the radius of the field of view will of course be smaller than the radius of rotation. Thus, only a central part of the sensitivity maps depicted in Figs 4-6 will be used.

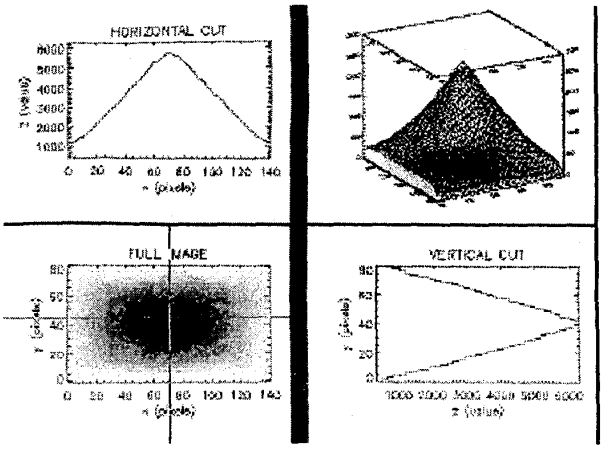

Fig. 4: Sensitivity map for a dual-headed configuration. X-axis is transaxial, Y-axis axial

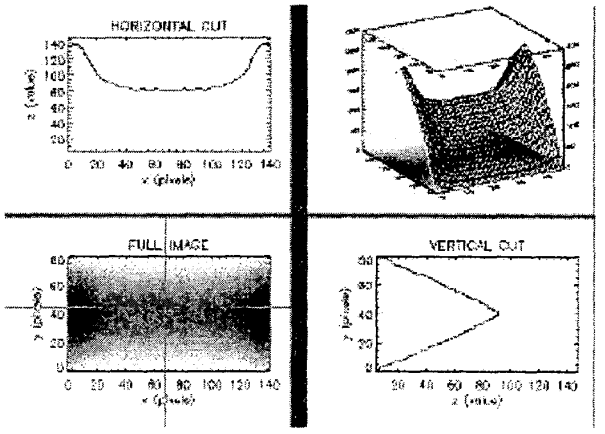

Fig. 5: Sensitivity map for a U-shaped configuration. X-axis is transaxial, Y-axis axial

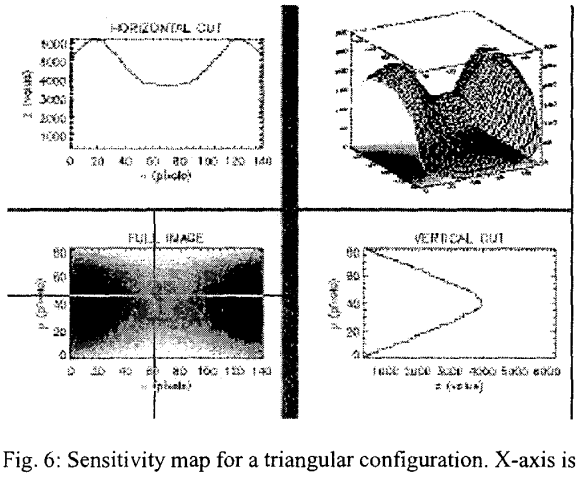

Fig. 6: Sensitivity map for a triangular configuration. X-axis is transaxial, Y-axis axial

We can see from these figures that in the central axial slice, the sensitivity is similar to the 2D sensitivity previously calculated [4]. The profile decreases quasi-linearly with increasing axial distance to the COR, as could be expected.

We also calculated a sensitivity map for a triangular system with the use of axial septa. These septa effectively constrain the axial angle of incidence of the LOR on the detector. This was simulated in our calculations by constraining the axial incidence angles to a maximum of 9°. The resulting map for this calculation is given in Figure 7.

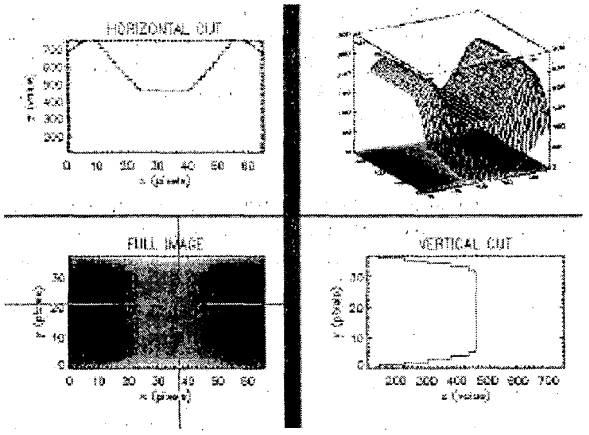

Fig. 7: Sensitivity map for a triangular configuration with axial septa. X-axis is transaxial, Y-axis axial

IV. Discussion

For a two-headed system, the sensitivity calculation results in a profile decreasing linearly in both the axial and the transaxial direction, as was already known from the literature [1]. The U-shaped transaxial profile gives a reasonably flat sensitivity profile in the transaxial direction. In this configuration, the added sensitivity by the third head compensates for the sensitivity decrease away from the center for the two opposing heads. Due to the tangential shift of the opposing heads, the sharp peak in the sensitivity at the center, as seen in the dual head case, is flattened. At the transaxial edges of FOV, the sensitivity increases, but in a real imaging environment the FOV is always less than the radius of rotation. The triangular configuration shows a decreasing sensitivity towards the center of the FOV. As mentioned in earlier work [4], this decrease is even more severe as the radius of rotation is increased, because this leads to an increasing gap between the detector heads. When the heads are placed more closely together, however, as is possible with the system under study, this decrease in the center of the FOV is not observed, and, in fact in those cases the triangular configuration gives the highest sensitivity.

One of the ways to account for the three-dimensional sensitivity variations is to calculate independent profiles for the sensitivity variation in the axial and the transaxial direction, and then multiply the two correction factors. For the case of dual-head coincidence imaging, this may be a reasonable approach. Indeed, Fig 4 shows that the shape of the transaxial sensitivity profile remains reasonably constant when moving axially through the sensitivity map. However, Figs 5 and 6, indicate that this approach might not give accurate results for triple-headed coincidence detection. Indeed, one can observe that the shape of the transaxial sensitivity profile varies when moving axially, an effect which can not be accounted for when using two separate correction profiles.

Concerning the calculations with the use of axial septa by restricting the axial angle of incidence, one can observe that at the central slice, the profile is similar as in the fully 3D case. As expected, the profile becomes much flatter in the axial direction, but will eventually fall to zero at the edges of the detector.

Additional work will be done on both real and simulated data to corroborate these results. We will also further investigate the separability of the obtained sensitivity maps.

V. Conclusions

We present here a method for the calculation of the three-dimensional geometric sensitivity for any camera configuration. The method was then applied to three realistic camera configurations. From the calculations, it becomes clear that the sensitivity correction can not be split into a transaxial and an axial correction, both directions have to be considered jointly. The use of axial septa results in a much flatter axial sensitivity profile. In this case, the two-dimensional approximation works reasonably well for the central region of the FOV.

VI. Acknowledgments

This work was supported by "Institute for the Promotion of Innovation by Science and Technology in Flanders" (IWT, Belgium).

Rik Van de Walle is a post-doctoral fellow of the Fund for Scientific Research-Flanders (FWO, Belgium).

VII. References

[1] A. Reader et al.; Fast accurate iterative reconstruction for low-statistics positron volume imaging: Phys. Med. Biol. 43 (1998) 835-846

[2] C.G. Matthews; Triple-Head Coincidence Imaging: presented at IEEE MIC, 1999, Seattle, USA

[3] S. Vandenberghe et al. ; Physical evaluation of 511 keV imaging with gamma camera and PET; presented at IEEE MIC, 1999, Seattle, USA

[4] Y. D'Asseler et al. ; Geometric sensitivity calculation of three-headed gamma camera-based coincidence detection., Presented at SPIE Medical Imaging 2000, San Diego, USA

[5] The IRIX gamma camera is manufactured by Marconi Medical Systems, 595 Miner Road, Cleveland, Ohio 44143, USA

[6] W. Swan : Exact Rotational Weights for Coincidence Imaging with a continuously rotating Dual-Headed gamma camera; presented at IEEE MIC, 1999, Seattle, USA